Spectrochimica Acta Part A: Molecular and Biomolecular Spectroscopy 169 (2016) 216–222

Contents lists available at ScienceDirect

Spectrochimica Acta Part A: Molecular and Biomolecular Spectroscopy

journal homepage: www.elsevier.com/locate/saa

Detection of *Citrus tristeza virus* by using fluorescence resonance energy transfer-based biosensor

Taha Roodbar Shojaei [a,*], Mohamad Amran Mohd Salleh [b,*], Kamaruzaman Sijam [c], Raha Abdul Rahim [d], Afshin Mohsenifar [e], Reza Safarnejad [f], Meisam Tabatabaei [g]

[a] Institute of Advanced Technology (ITMA), Universiti Putra Malaysia, 43400 Serdang, Selangor, Malaysia
[b] Department of Chemical and Environmental Engineering, Faculty of Engineering, Universiti Putra Malaysia, 43400 Serdang, Selangor, Malaysia
[c] Department of Plant Protection, Universiti Putra Malaysia, 43400 Serdang, Selangor, Malaysia
[d] Department of Cell and Molecular Biology, Faculty of Biotechnology and Biomolecular Sciences, Universiti Putra Malaysia, 43400 Serdang, Selangor, Malaysia
[e] Research and Development Department, Nanozino, 16536-43181 Tehran, Iran
[f] Department of Plant Viruses, Iranian Institute of Plant Protection, Tehran, Iran
[g] Nanosystems Research Team (NRTeam), Microbial Biotechnology and Biosafety Dept., Agricultural Biotechnology Research Institute of Iran (ABRII), Karaj, Iran

ARTICLE INFO

Article history:
Received 1 January 2016
Received in revised form 12 June 2016
Accepted 28 June 2016
Available online 29 June 2016

Keywords:
Fluorometric immunoassay
Nanobiosensor
Cadmium-telluride quantum dots
Gold nanoparticles
Bioconjugation
Quenching

ABSTRACT

Due to the low titer or uneven distribution of *Citrus tristeza virus* (CTV) in field samples, detection of CTV by using conventional detection techniques may be difficult. Therefore, in the present work, the cadmium-telluride quantum dots (QDs) was conjugated with a specific antibody against coat protein (CP) of CTV, and the CP were immobilized on the surface of gold nanoparticles (AuNPs) to develop a specific and sensitive fluorescence resonance energy transfer (FRET)-based nanobiosensor for detecting CTV. The maximum FRET efficiency for the developed nano-biosensor was observed at 60% in AuNPs-CP/QDs-Ab ratio of 1:8.5. The designed system showed higher sensitivity and specificity over enzyme linked immunosorbent assay (ELISA) with a limit of detection of 0.13 μg mL^{-1} and 93% and 94% sensitivity and specificity, respectively. As designed sensor is rapid, sensitive, specific and efficient in detecting CTV, this could be envisioned for diagnostic applications, surveillance and plant certification program.

1. Introduction

Citrus tristeza virus (CTV) as a phloem-limited *Closterovirus* is distributed all over the world and acts as a causal agent of one the most destructive disease named tristeza disease [1]. CTV infects almost all citrus species leading to a significant economic losses in the citrus industry [1]. Efficient seed and plantlet certification programs are the most important way to control spreads of CTV infection. Therefore, developing accurate and reliable detection techniques capable of detecting viruses in early stages of infection is of crucial importance. To date, different techniques have been used to detect CTV including biological indexing [2], serological and immunoassay techniques [3] as well as polymerase chain reaction (PCR)-based techniques [4]. These conventional detection techniques generally suffer from different drawbacks and therefore, there is a growing demand for developing simpler and more rapid, detection method which offers higher sensitivity and specificity as well [5].

By the introduction of nanosciences in the last decade, broad kinds of nanoscale materials with exclusive features have attracted a great deal of attention for disease diagnosis. From those nanoscale materials, quantum dots (QDs) owing to their unique characteristics such as easy synthesis and handling, long shelf life, high fluorescence yields, high resistance to photo-bleaching, and narrow symmetric emission spectrum have been widely used in fluorescence resonance energy transfer (FRET)-based sensors as an ideal donors for sensitive and rapid detection of different types of diseases [6–10]. It is worth quoting that QDs are generally composed of different semiconductor elements which have smaller sizes than the exciton Bohr radius [11].

On the other hand, different kinds of chemical materials and nanoparticles have been used as acceptor in the FRET-based sensors including rhodamine [6,8], TAMRA [7], gold nanoparticles [12,13], graphene oxide [14] and carbon nanotubes [15]. Among the above-mentioned materials, gold nanoparticles (AuNPs) offers unique optical properties and as a result, they have been used widely for detecting different

* Corresponding authors.
E-mail addresses: tahashojaee2000@yahoo.com (T.R. Shojaei), asalleh@upm.edu.my (M.A.M. Salleh).

http://dx.doi.org/10.1016/j.saa.2016.06.052
1386-1425/

analysts [12,16]. In fact, AuNPs have been considered as excellent FRET-based quencher because of their plasmon resonances in the visible range [17].

By considering the significance of the FRET phenomenon in clinical applications, great deals of theoretical and experimental researches have been performed to investigate the influence of metal surface on the emission spectra of fluorophore molecules [18,19]. In fact, a fluorophore molecule in the vicinity of a metal nanoparticle shows a wide-range of fluorescence dependency on the distance between fluorophore and nanoparticle [20].

Having elaborated that, the present study was set to take advantage of AuNPs as an acceptor placed in the vicinity of QDs to develop a sensitive, simple, and rapid FRET-based nanobiosensor for CTV detection. More specifically, a detection strategy was designed by labeling specific antibody against CTV's coat protein (CP) with QDs (QDs-Ab) while the target proteins (CP) were labeled with AuNPs (AuNPs-CP). The AuNPs-labeled CP and QDs-labeled antibody formed an immuno-complex. Therefore, the proximity of the QDs and AuNPs led to an energy transfer between the donor and the acceptor which consequently resulted in decreased fluorescence intensity of the QDs. At the detection stage and in the presence of target proteins in a given sample, the AuNPs-CP was competitively replaced by free CPs resulting in a recovery of the fluorescence intensity of the QDs.

2. Material and methods

2.1. Plant materials

Field samples were collected in January 2014 from different citrus trees growing in different orchards in Selangor and Pahang states of Malaysia. The young leaves from four different locations around the canopy pointing east, west, south, and north were collected in plastic bags, marked, and stored in a dry ice box and were then stored at −20 °C until use.

2.2. CTV presence confirmation

The presence and confirmation of CTV was performed at the plant protection department of the agricultural research institute by using reverse transcription polymerase chain reaction (RT-PCR).

2.3. Sap extraction from plant materials

The extraction of plants sap from healthy and infected citrus trees was carried out by crushing 1 g leaves in liquid nitrogen followed by suspension in 500 μL Tris-HCl buffer (70%, pH 7.5) (Thermo Fisher Scientific Inc.). The sap was then stored at −20 °C for future experiments.

2.4. ELISA procedure

The ELISA was performed as a standard test using a Bioreba ELISA Kit (Bioreba) following the manufacture protocol with some modification in order to compare with the sensitivity and specificity of the FRET-based nanosensor developed in the present study. Briefly, the 96-wells microtiter plate (Thermo Fisher Scientific Inc.) was coated with 100 μL of anti-CP antibody diluted to 1:500 in phosphate buffered saline (PBS) using carbonate coating buffer, and the plate was then incubated at 37 °C for 2 h. The plate was washed with PBST (PBS containing 0.05% (v/v) Tween-20) three times. The extracted sap samples obtained from the infected and healthy plant materials, as well as a known negative sample (as negative control), i.e., a sample infected with witches' broom disease of lime (WBDL), and purified CP protein (as positive control) were added to the plate in three replicates and the plate was left overnight at 4 °C. Then, it was washed with PBST as described above. Afterwards, diluted alkaline phosphatase-conjugated goat anti-rabbit IgG (Abcam, UK) was added to each well and the plate was incubated at 37 °C for 2 h. Subsequently, the para-Nitrophenylphosphate (pNPP) (Sigma-Aldrich) as substrate was added to the plate followed by incubation for 30 min and finally, absorbance reading was performed.

2.5. Limit of detection (LOD) of ELISA

The LOD was estimated by analyzing ten samples with known CP concentrations (1 to 10 μg mL^{-1} CP) and a blank sample in six replications based on the procedure described above. Then, the standard deviation was calculated from the replications of the blank sample and the slope of the calibration curve was measured from the standard samples with the known concentrations. Afterwards, the LOD was estimated by using the following equation (Eq. (1)):

$$\mathrm{LOD} = 3S_0/K \tag{1}$$

where S_0 is the standard deviation of blank measurements (n = 6) and K is the slope of calibration curve.

2.6. Synthesis of thiolglycolic acid capped CdTe QDs

The water-soluble CdTe QDs were synthesized by using the procedure reported in our previous study [21]. In brief, 0.1 g Te powder was reduced by 0.3 g NaBH4 in 10 mL double-distilled water under stirring at 80 °C for 3 h. Then, a freshly prepared NaHTe solution was added gradually to N_2-saturated $CdCl_2 \cdot 2.5H_2O$ (Sigma-Aldrich) solution (0.4 g $CdCl_2$ in 100 mL double-distilled water) at pH 10 in the presence of 250 μL thiolglycolic acid (TGA) (Sigma-Aldrich). The mixture solution was heated at 92 °C and stirred in a reflux system under nitrogen gas. The crude solution was then precipitated and washed three times with ethanol and centrifuged for 15 min at 4000 × *g*. The precipitate was re-dispersed in 250 mL double distilled water and stored at 4 °C in the dark.

2.6.1. Labeling of antibody with QDs

In order to label the antibody with QDs, 400 μL of QDs and 200 μL of freshly prepared 1-ethyl-3-(3 dimethylaminopropyl)-carbodiimide (EDC) (Sigma-Aldrich) (6.4 mg mL^{-1}) and N-hydroxysuccinimide (NHS) (Thermo Fisher Scientific Inc.) (4.5 mg mL^{-1}) were mixed and incubated in a dark water bath at 37 °C for 1 h. Afterwards, 60 μL of the purified polyclonal antibodies (0.25 mg mL^{-1}) was added drop-wise to the solution in the dark and stirred gently at 4 °C for 2 h. Subsequently, 540 μL tris buffer (6 mg mL^{-1}, pH 7.2) was added to the solution and stirred under the above-mentioned condition for 1 h. The mixture was then centrifuged at 18,900 × *g* at 4 °C for 10 min. The lower phase was removed and the upper phase containing the QDs-labeled antibodies (QDs-Ab) were diluted by 1200 mL tris buffer and stored at 4 °C until use. To confirm successful conjugation of the QDs and the antibody, spectrophotometeric analysis was performed.

2.7. Synthesis of AuNPs

AuNPs were synthesized by the citrate reduction method by mixing 1 mL tri-sodium citrate (Sigma-Aldrich) solution (37.5 mg in 1 mL distilled water) to 5 mg $HAuC1_4 \cdot 3H_2O$ (Sigma-Aldrich) in 48 mL distilled water under stirring at 70 °C until the solution turned red.

2.7.1. Labeling of antigen with AuNPs

In order to label the antigen with the AuNPs, 400 μL of AuNPs and 200 μL of freshly prepared EDC (6.4 mg mL^{-1}) and NHS (4.5 mg mL^{-1}) were mixed and incubated in a water bath at 37 °C for 1 h. Afterwards, 30 μL of CP (0.25 mg mL^{-1}) were added drop-

wise to the solution and stirred gently at 4 °C for 2 h. Subsequently, 570 μL tris buffer (6 mg mL^{-1}, pH 7.2) was added to the solution and stirred under the above-mentioned condition for 1 h. The separation of excess substances from the AuNPs-CP conjugate mixture was performed through overnight dialysis against tris buffer by using dialysis tubing cellulose membrane (Sigma-Aldrich, 27 mm). Successful conjugation of AuNPs and antigen was investigated by Spectrophotometry as well.

2.8. Determination of FRET quenching efficiency

The FRET quenching efficiency (E) was estimated by using the Eq. ((2), where F and F_0 are the fluorescence intensity of the donor in the presence and absence of the acceptor, respectively. In order to determine the best FRET efficiency, varying concentrations of AuNPs-CP (0.2 to 0.9 nM) were added to a constant concentration of QDs-Ab (6 nM) in sequence. In another word, different AuNPs-CP/QDs-Ab ratio of 1:6.5, 1:7.5, 1:8.5, 1:10, 1:12, 1:15, 1:20 and 1:30 were tested by using spectrofluorometer.

$$E = 1\text{-}(F/F_0) \tag{2}$$

2.9. The positive cut-off value determination

The positive cut-off value of the developed nanobiosensor was investigated by analyzing a negative control in six replications by using $\overline{X} + 3SD$.

Where X is the average fluorescence intensity value of the negative control and SD is the standard deviation. Samples whose fluorescence intensity was above this value were considered positive. The positive cut-off value of the ELISA was investigated by analyzing six replications of the negative control and the optical density (OD) of the samples was monitored.

2.10. Nanobiosensor evaluation and determination of LOD

To evaluate the capability of the developed nanobiosensor in detection of CTV, 9 μL QDs-Ab were added to 488 μL tris buffer (6 mg mL^{-1}, pH 7.2). Then 1.92 μL of AuNPs-CP was added to the solution and incubated for 3 min to ensure that the immuno-complex of the QDs-Ab and AuNPs-CP was formed. The solution was then excited at 370 nm and emission spectra (450 to 750 nm) were recorded. Afterwards, artificially-contaminated samples (0.1 to 1 μg mL^{-1} CP) were sequentially added to the reaction mixture containing QDs-Ab and AuNPs-CP and incubated for 5 min. In addition, the specificity of the nanobiosensor was also tested by using four witches' broom disease of lime (WBDL) infected samples. The solution was excited at 370 nm and the baseline curve was recorded. Maximum excitation and emission wavelength were recorded at 370 and 565 nm, respectively. Both excitation and emission slits were 5 nm.

The LOD was estimated by analyzing ten samples with known CP concentrations (0.1 to 1 μg mL^{-1} CP) and the blank sample in six replications following the same procedure used for ELISA.

2.11. Detection of field samples by using nanobiosensor

In the detection step, to determine the ability of the designed nanobiosensor in detection of field samples, 5 μL plant midrib from 15 CTV infected samples and 17 healthy samples were tested by spectrofluorimetry as previously mentioned. The sample was marked as negative when no or negligible baseline shift was observed but if the baseline was recovered, the sample was considered as positive.

2.12. Data analysis

The sensitivity and specificity of both diagnostic techniques were calculated using the following formula (Eqs. ((3) and ((4), respectively).

$$\text{Sensitivity} = \frac{\text{True Positive}}{\text{True Positive} + \text{False Negative}} \times 100 \tag{3}$$

$$\text{Specificity} = \frac{\text{True Negative}}{\text{True Negative} + \text{False Positive}} \times 100 \tag{4}$$

2.13. Characterizations

All spectrophotometeric analysis was carried out using a Perkin-Elmer Lambda 35 UV–vis spectrometer (USA). In this step, 500 μL from each sample was added to a 5 mm quartz cuvette individually while 1 mL water was added to the other cuvette as a blank sample. All fluorometric studies were performed by using a Shimadzu, RF-5301PC Spectrofluorophotometer (Japan). The synthesized nanoparticles were characterized by using transmission electron microscope (TEM) (Hitachi H-7100 TEM) and fourier transform infrared (FTIR) spectroscopy (Thermo Nicolet, Smart Orbit, FTIR Nexus) and the particle diameter size was determined using the ImageJ software (Version 1.46r, National Institute of Health, USA). For TEM analysis, 30 μL from synthesized nanoparticles were dropped on copper TEM grids. Then, the grids were dried at room temperature and tested by TEM. To carry out FTIR analysis, 20 μL from each sample was placed individually on the surface of FTIR sample reader and the reader was pushed down to touch the sample and the absorption bands were recorded at room temperature.

3. Results

The cut-off value of the ELISA was estimated using the six replications of the negative control at 0.329 + 0.373 a.u. and the samples whose absorbance value was above this value were considered as positive. In the ELISA test, 12 out of 15 samples were found positive (infected) and 15 out of the 17 negative samples were detected as non-infected (Table 1). In addition, two infected samples that were detected as positive by the nanobiosensor assay were reported negative by the ELISA method (Table 1). Therefore, it could be concluded that the sensitivity and specificity of the ELISA for detecting CTV were at 80% and 88%, respectively.

As presented in Fig. 1, the TEM images of the QDs and AuNPs showed that the prepared nanoparticles had a spherical morphology and good monodispersity with a particle size of about 4 nm and 27 nm, respectively.

The QDs exhibited the characteristic absorption bands associated with the O—H stretching vibrations at 3429 cm^{-1}, C—H stretching vibrations at 2925 cm^{-1}, 2858 cm^{-1} and 1511 cm^{-1}, C—N stretching vibrations at 1381 cm^{-1} and 1242 cm^{-1}, C═O stretching vibrations at 1739 cm^{-1} and 1050 cm^{-1} and C—C stretching vibrations at 1632 cm^{-1} (Fig. 2). The AuNPs exhibited characteristic absorption bands associated with the O—H stretching vibrations at 3495 cm^{-1}, S—H stretching vibrations at 2433 cm^{-1}, C═O stretching vibrations at 1770 cm^{-1}, C—C stretching vibrations at 1658 cm^{-1}, S—O stretching vibrations at 1365 cm^{-1} and C—Cl stretching vibrations at 617 cm^{-1} (Fig. 2).

To probe the potentials of QDs and AuNPs as donor and acceptor pairs, the absorption and emission spectra of the pure solutions of AuNPs and QDs were monitored. The maximum emission peak of the QDs was obtained at 565 nm, while the maximum absorption peak of the AuNPs was estimated at 527 nm. Therefore, the emission wavelength of the QDs and absorption wavelength of the AuNPs showed

Table 1
Detection results of analyzed field samples by using developed nanobiosensor and ELISA including 15 CTV infected samples, 17 healthy samples and four WBDL infected samples.

Sample category	Sample number	DAS-ELISA[a] (light absorbance)	AuNP sensor[b] (a.u.)
CTV-infected samples	1	0.60	0.54
	2	2.01	0.65
	3	1.21	0.50
	4	0.78	0.47
	5	1.03	0.63
	6	0.69	0.43
	7	0.72	0.49
	8	1.05	0.51
	9	0.90	0.48
	10	0.56	0.40
	11	1.43	0.52
	12	0.88	0.50
	13	2.27	0.62
	14	1.63	0.54
	15	0.91	0.46
CTV-non-infected samples	1	0.14	0.35
	2	0.25	0.40
	3	0.84	0.42
	4	0.12	0.31
	5	0.30	0.33
	6	0.10	0.40
	7	0.19	0.31
	8	0.57	0.38
	9	0.11	0.30
	10	0.10	0.40
	11	0.64	0.30
	12	0.21	0.40
	13	0.32	0.37
	14	0.71	0.39
	15	0.27	0.30
	16	0.16	0.37
	17	0.47	0.40
WBDL-infected samples	1	0.19	0.38
	2	0.46	0.32
	3	0.10	0.37
	4	0.54	0.40

[a] Absorbance measured at OD_{405}. Standard deviation was estimated at 0.538.
[b] Baseline estimated by adding samples to the solution containing QD-Ab and AuNPs-CP. Standard deviation was estimated at 0.094.

maximum spectral overlap which is critical to achieve an efficient FRET phenomenon (Fig. 3).

To verify the attachment of the antibodies and antigens to the surface of the QDs and the AuNPs, respectively, the spectrophotometric analysis was performed. As seen in Fig. 4, the maximum peaks for bare and conjugated QDs were recorded in 548 nm and 551 nm, respectively. The maximum OD values for un-conjugated and conjugated QDs were recorded at 0.42 a.u. and 0.32 a.u., respectively. The maximum peak shifts to longer wavelength (red-shift) and the OD decrease of the QDs-Ab confirmed successful covalent coupling between the antibody and the QDs. Moreover, the OD of the AuNPs-CP was reduced in comparison with the pure AuNPs revealing the attachment of the antigens to the surface of the AuNPs. In addition, the spectral position of the AuNPs extinction peak (λ_{max}) was altered from 527 nm to 540 nm when bare and conjugated AuNPs were tested, respectively (Fig. 5).

The FRET efficiency (E), directly dependent on the AuNPs-CP/QDs-Ab ratio, was estimated using the Eq. ((2). The maximum FRET efficiency for the developed nano-biosensor was observed at AuNPs-CP/QDs-Ab ratio of 1:8.5, while the FRET efficiency decreased by using higher ratios and kept constant by using lower ratios (Fig. 6).

The cut-off value was set at 0.407 + 0.012 a.u. to differentiate the healthy and infected samples. The standard deviation was estimated by testing the blank sample in six replications. Samples whose fluorescence intensity was measured above this value were considered positive.

On account of the cut-off value, the developed nanobiosensor successfully detected 14 out of the 15 positive samples as infected while it identified 16 out of the 17 healthy samples as negative (Table 1). All four WBDL infected samples were found negative as well. Therefore, the nanobiosensor detected CTV with 93% and 94% sensitivity and specificity, respectively without any cross reactivity with WBDL (Table 1).

The two conjugates, QDs-Ab and AuNPs-CP, were further conjugated based on the antibody–antigen interaction phenomenon. The hybridization between QDs-Ab and AuNPs-CP led to FRET phenomena. The emission spectrum of the solution containing both QDs-Ab and AuNPs-CP showed a significant decrease in the fluorescence intensity. Herein, when an infected sample was added to the reaction mixture, a significant increase was observed in the fluorescence intensity of the solution (Fig. 7).

The emission intensity of the QDs-Ab at a λ_{max} of 565 nm was increased upon the addition of free CP from 0.1 μg mL^{-1} to 1 μg mL^{-1}. Therefore, it could be concluded that shifts in the emission of the QDs-Ab were directly related to the final concentration of the CP. Further increases in CP led to insignificant augmentation in the emission peak of QDs-Ab (Fig. 8).

By using the Eq. (1), the LOD of the developed system was obtained at 0.13 μg mL^{-1} (130 ng mL^{-1}) (the standard curve was linear with a

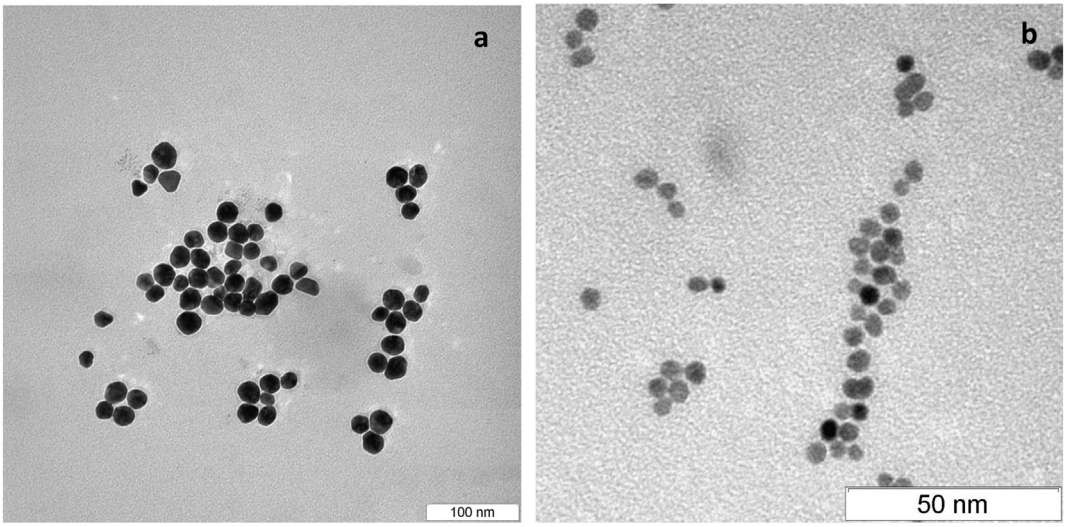

Fig. 1. TEM images of synthesized AuNPs (a) and QDs (b).

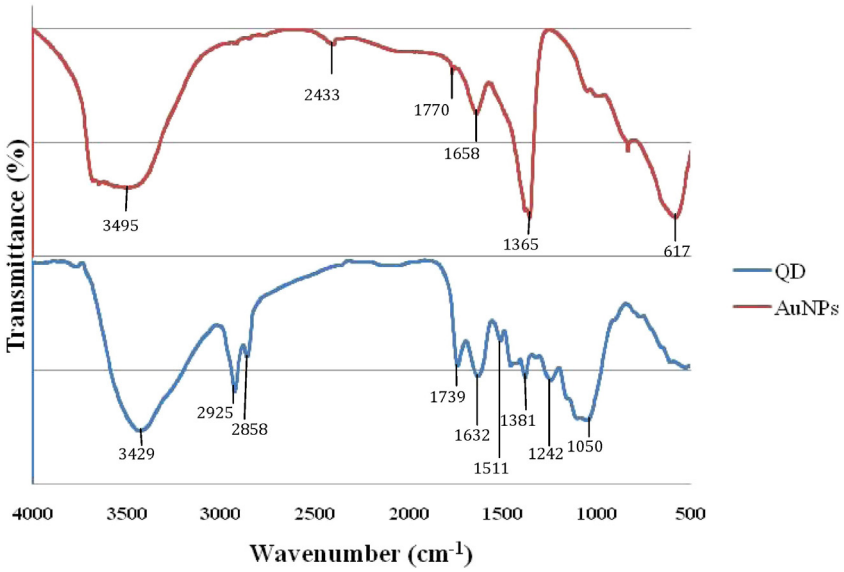

Fig. 2. FTIR spectrum of AuNPs and QDs.

correlation coefficient $R^2 = 0.98$), while the LOD for ELISA was estimated at 2.85 μg mL^{-1} (2850 ng mL^{-1}) ($R^2 = 0.91$).

4. Discussion

In the present study, a FRET-based nanobiosensor was developed to detect CTV using AuNPs and QDs conjugated with CP and antibody, respectively. AuNPs/QDs FRET-based nanobiosensors have been used in the detection of a number of ions, pathogens, nucleotides, and molecules earlier [12,22–24]. Nevertheless, to the best of our knowledge, this is the first effort to develop such nano-based system for detecting CTV using the AuNPs immobilized with target proteins and the antibodies labeled with QDs.

On account of the fact that CP, the protein product of ORF3, has been widely used in the detection of CTV [3,4,25,26], therefore, in this study, the CTV detection was also performed based on the CP region of CTV.

ELISA technique has been probably employed with CTV more than with any other plant virus [1] and has demonstrated an appropriate limit of detection [26]. Moreover, that official methods including the mandatory control program now relies on this method [27]. Therefore, in the present study the newly developed nanosensor was compared with ELISA as a gold standard technique for detecting CTV.

Despite the false negative results obtained in the ELISA, this technique was able to differentiate CTV and WBDL. The false negative and false positive results obtained in the ELISA were in the context of the viral concentration in the leaves used as well as the uneven distribution of the viruses in different plant parts. The critical effect of viral concentration in samples and low quantity of virus in leaves have been proven in previous studies [4,28,29]. Moreover, the observed sensitivity and specificity of 80% and 88%, respectively, were in agreement with those of the previous studies based on which they concluded that ELISA could be a suitable technique for detecting CTV [25,27,29,30].

Characterization of the spherical prepared water-soluble QDs and AuNPs by TEM confirmed that the synthesized particles were appropriate to be used in the nanobiosensor. Moreover, the FTIR results revealed that QDs and AuNPs were probably water soluble materials with a large number of hydroxyl, carbonyl, or carboxylic acid groups on their surfaces. This large number of hydroxyl, carbonyl, or carboxylic acid groups on the surface of QDs indicated that the QDs were successfully bound to the carboxylic acid functional group of TGA.

As seen in Fig. 3, the emission wavelength of the QDs and absorption wavelength of the AuNPs had an appropriate overlap. Therefore, QDs

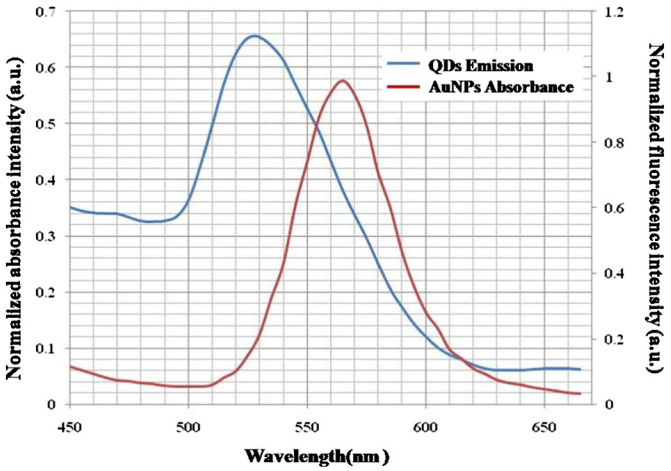

Fig. 3. Overlap between QDs emission spectrum and AuNPs absorption spectrum.

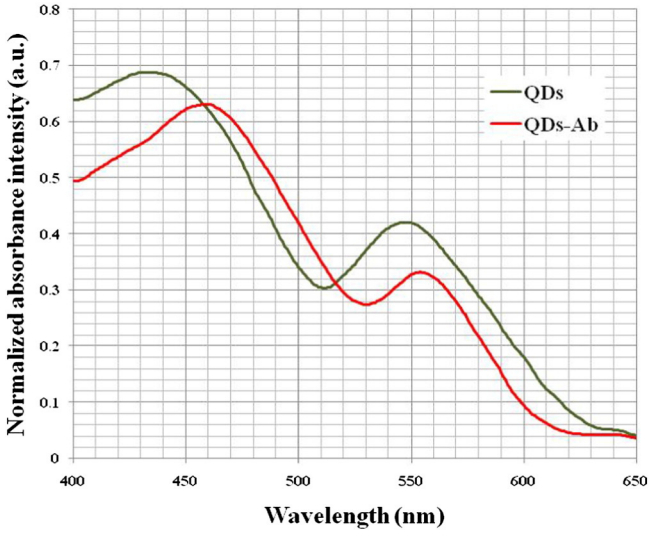

Fig. 4. Absorbance intensity of bare QDs and antibody immobilized-QDs (QDs-Ab).

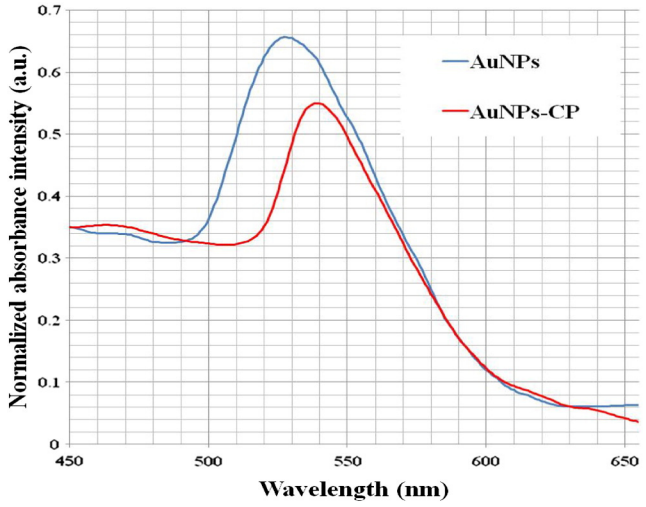

Fig. 5. Absorbance intensity of bare AuNPs and coat protein immobilized-AuNPs (AuNPs-CP).

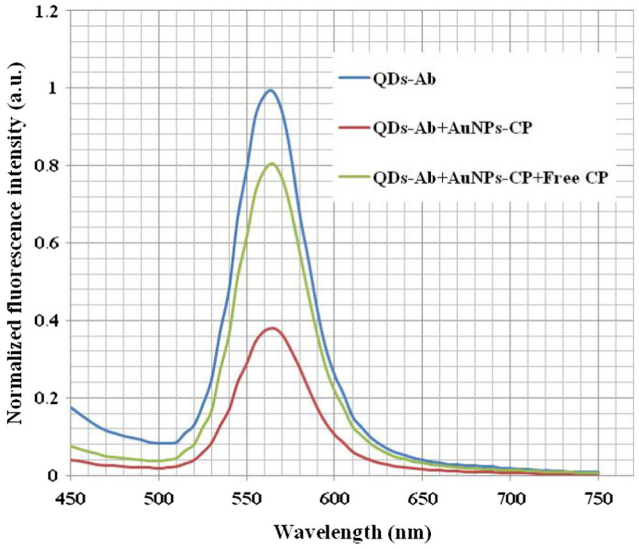

Fig. 7. Fluorescence spectrums of solution containing QDs-Ab, QDs-Ab + AuNPs-CP and solution containing QDs-Ab + AuNPs-CP + free CP achieved by using spectrofluorometer.

and AuNPs could be chosen as suitable donor and acceptor, respectively, in fabricating nanobiosensors. The capability of AuNPs as acceptor in the QDs FRET mechanism was in agreement with the findings of other researchers who also used AuNPs as acceptor to quench QDs [12,22,31].

The maximum peak shifts to longer wavelength (red-shift) and the decreases in the OD of the conjugated QDs and AuNPs compared with the bare QDs and AuNPs confirmed the successful covalent coupling between the antibody and antigen to the nanoparticles. Attachment of bio-molecules to the surface of the nanoparticles has reportedly altered the local refractive index, leading to changes in the λ_{max} of nanoparticles [32]. The observed decrease in OD and maximum peak shifts in the conjugated nanoparticles were in agreement with the results previously obtained by other researchers [7,32]. The antibodies were immobilized on the surface of QDs via covalent interactions between carboxyl groups of the TGA-capped QDs and amino groups of the antibody. Besides, the existence of free amine groups (arginine or lysine) in the antigens led to an effective attachment of the CP antigen to AuNPs via interactions between carboxyl groups of AuNPs and amine groups of CP. Above all, the carboxylic group existed on the surface of QDs and AuNPs was activated by using EDC/NHS chemistry to create a reactive ester intermediate with the carboxylic group. The reactive ester roles as a cross-linker and could be attached covalently to the amine groups of the antibodies and antigens. The remaining activated domains were then blocked by using tris buffer.

To determine the optimum FRET signal between the QDs and AuNPs, different ratios of AuNPs-CP/QDs-Ab were tested during the nanobioconjugate preparation. The optimum FRET signal was obtained at AuNPs-CP/QDs-Ab ratio of 1:8.5. At this ratio, the attachment of a suitable amount of AuNPs-CP on the surface of QDs-Ab was achieved. At higher ratios, overloaded QDs-Ab did not participate in the formation of the immunocomplex. As a result the excess QDs-Ab reacted with free CP in the samples (data not shown). This would principally endanger the developed system when lower concentrations of CP existed in the specimen and subsequently no considerable shifts in FRET signals occurred. On the other hand, at lower ratios, thanks to the presence of the excess AuNPs-CP, higher value of CP were needed to overcome the competitive replacement in binding sites of the antibodies immobilized on the surface of QDs. This led to loss of the accuracy and the sensitivity of the nanobiosensor in the detection of lower concentrations of CP in specimens.

Due to the fact that the attachment of antibody to the antigen is not a rugged kind; so, in the current study when the free CP was added to the reaction mixture containing both QDs-Ab and AuNPs-CP, the AuNPs-CP was replaced by the free CP. This resulted in an upward change in the fluorescence intensity compared with the fluorescence intensity formerly recorded for the solution containing both QDs-Ab and AuNPs-CP. The AuNPs-CP optically quenched the QDs-Ab based on the Forster

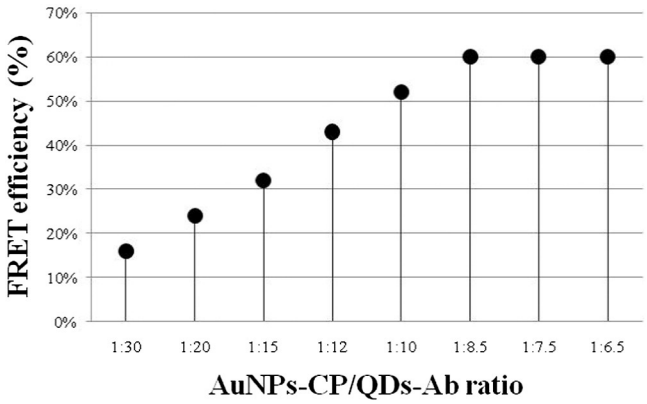

Fig. 6. FRET efficiency of AuNPs for different ratios of AuNPs-CP to QDs-Ab.

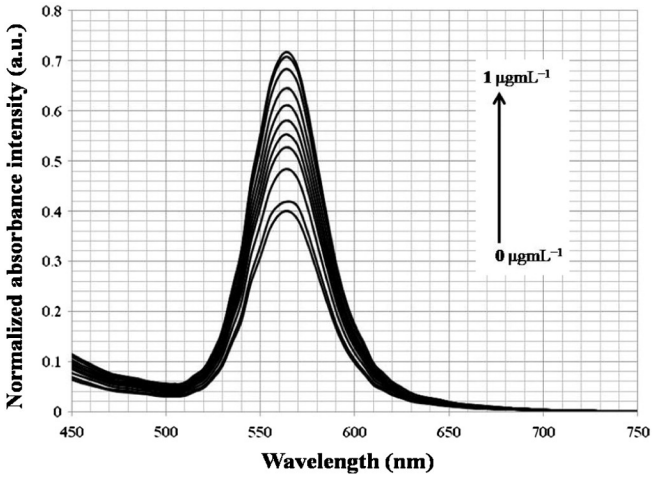

Fig. 8. The effect of different concentrations of CP varying from 0 to 1 μg mL^{-1} on the fluorescent intensity of QDs.

dipole–dipole interaction form [33]. More especially, the AuNPs-CP as a fluorescence acceptor attached to the antigen protein (CP) occupied the antibodies immobilized on the surface of QDs resulting in a FRET signal. In the presence of the free CP, the free CP displaced the AuNPs-CP domain in the reaction mixture and led to the fluorescence recovery of the conjugated QDs-Ab.

The detection limit of the nanobiosensor was twenty times higher than that of ELISA. This result was in agreement with those reported by other researchers [6,8]. Moreover, AuNPs/QDs-based sensor developed in this study showed lower detection limit over carbon nanoparticles/QDs-based sensor for detecting CTV [26]. Consequently and based on the results achieved herein, it was possible to monitor even very low concentrations of CP in the specimens by comparing the obtained signals with the standard curve.

5. Conclusions

By considering the smaller amount of sample required in the developed nanobiosensor, it could be an appropriate method where limited volumes of sample are available. On the other hand, although ELISA could be used in detection procedures, unlike nanosensors such systems are time-consuming and not relatively easy to handle as they need various reagents and washing steps. In addition, the better detection limit observed for the nanobiosensor developed herein compared with that of ELISA marked the AuNPs/QDs nanobiosensor as a suitable technique for seedling screening programs where plants might be at the first stage of infection. Moreover, the developed nanobiosensor could detect samples within a few minutes and therefore, it could be of great preference during large scale screening programs.

Conflict of interest

The authors declare that they have no conflict of interests.

References

[1] P. Moreno, S. Ambrós, M.R. Albiach-Martí, J. Guerri, L. Pena, Citrus tristeza virus: a pathogen that changed the course of the citrus industry, Mol. Plant Pathol. 9 (2008) 251–268, http://dx.doi.org/10.1111/J.1364-3703.2007.00455.X.
[2] C.N. Roistacher, Graft-transmissible diseases of citrus, Handb. Detect. Diagnosis, Food and Agriculture Organization of the United Nations, Rome, Italy, 1991.
[3] M. Cambra, M.T. Gorris, M.P. Román, E. Terrada, S.M. Garnsey, E. Camarasa, A. Olmos, M. Colomer, Routine detection of citrus tristeza virus by direct immunoprinting-ELISA method using specific monoclonal and recombinant antibodies, Proceeding 14th Conf. Int. Organ. Citrus Virol., Riverside, California 2000, pp. 34–41.
[4] C.R. Adkar-Purushothama, P.K. Maheshwar, T. Sano, G.R. Janardhana, A sensitive and reliable RT-nested PCR assay for detection of citrus tristeza virus from naturally infected citrus plants, Curr. Microbiol. 62 (2011) 1455–1459, http://dx.doi.org/10.1007/s00284-011-9883-7.
[5] T. Roodbar Shojaei, M. Tabatabaei, S. Shawky, M.A. Mohd Salleh, D. Bald, A review on emerging diagnostic assay for viral detection: the case of avian influenza virus, Mol. Biol. Rep. 42 (2015) 187–199, http://dx.doi.org/10.1007/s11033-014-3758-5.
[6] H. Safarpour, M.R. Safarnejad, M. Tabatabaei, A. Mohsenifar, F. Rad, M. Basirat, F. Shahryari, F. Hasanzadeh, Development of a quantum dots FRET-based biosensor for efficient detection of polymyxa betae, Can. J. Plant Pathol. 34 (2012) 507–515, http://dx.doi.org/10.1080/07060661.2012.709885.
[7] R. Zekavati, S. Safi, S.J. Hashemi, T. Rahmani-Cherati, M. Tabatabaei, A. Mohsenifar, M. Bayat, Highly sensitive FRET-based fluorescence immunoassay for aflatoxin B1 using cadmium telluride quantum dots, Microchim. Acta 180 (2013) 1217–1223, http://dx.doi.org/10.1007/s00604-013-1047-y.
[8] F. Rad, A. Mohsenifar, M. Tabatabaei, M.R. Safarnejad, F. Shahryari, H. Safarpour, A. Foroutan, Detection of candidatus phytoplasma aurantifolia with a quantum dots FRET-based biosensor, J. Plant Pathol. 94 (2012) 525–534, http://dx.doi.org/10.4454/JPP.FA.2012.054.
[9] W.R. Algar, U.J. Krull, Quantum dots as donors in fluorescence resonance energy transfer for the bioanalysis of nucleic acids, proteins, and other biological molecules, Anal. Bioanal. Chem. 391 (2008) 1609–1618, http://dx.doi.org/10.1007/s00216-007-1703-3.
[10] M.F. Frasco, N. Chaniotakis, Semiconductor quantum dots in chemical sensors and biosensors, Sensors 9 (2009) 7266–7286, http://dx.doi.org/10.3390/s90907266.
[11] J.M. Costa-Fernandez, Optical sensors based on luminescent quantum dots, Anal. Bioanal. Chem. 384 (2006) 37–40, http://dx.doi.org/10.1007/s00216-005-0189-0.
[12] T. Roodbar Shojaei, M.A. Mohd Salleh, M. Tabatabaei, A. Ekrami, R. Motallebi, T. Rahmani-Cherati, A. Hajalilou, R. Jorfi, Development of sandwich-form biosensor to detect mycobacterium tuberculosis complex in clinical sputum specimens, Braz. J. Infect. Dis. 18 (2014) 600–608, http://dx.doi.org/10.1016/j.bjid.2014.05.015.
[13] U. Uddayasankar, U.J. Krull, Energy transfer assays using quantum dot–gold nanoparticle complexes: optimizing oligonucleotide sssay configuration using monovalently conjugated quantum dots, Langmuir 31 (2015) 8194–8204, http://dx.doi.org/10.1021/acs.langmuir.5b01932.
[14] M. Liu, H. Zhao, X. Quan, S. Chen, X. Fan, Distance-independent quenching of quantum dots by nanoscale-graphene in self-assembled sandwich immunoassay, Chem. Commun. 46 (2010) 7909–7911, http://dx.doi.org/10.1039/c0cc02085k.
[15] S.M. Taghdisi, S.S. Emrani, K. Tabrizian, M. Ramezani, K. Abnous, A.S. Emrani, Ultrasensitive detection of lead (II) based on fluorescent aptamer-functionalized carbon nanotubes, Environ. Toxicol. Pharmacol. 37 (2014) 1236–1242, http://dx.doi.org/10.1016/j.etap.2014.04.020.
[16] A. Vaseghi, N. Safaie, B. Bakhshinejad, A. Mohsenifar, M. Sadeghizadeh, Detection of pseudomonas syringae pathovars by thiol-linked DNA–gold nanoparticle probes, Sensors Actuators B Chem. 181 (2013) 644–651, http://dx.doi.org/10.1016/j.snb.2013.02.018.
[17] N.-T. Chen, S.-H. Cheng, C.-P. Liu, J.S. Souris, C.-T. Chen, C.-Y. Mou, L.-W. Lo, Recent advances in nanoparticle-based förster resonance energy transfer for biosensing, molecular imaging and drug release profiling, Int. J. Mol. Sci. 13 (2012) 16598–16623, http://dx.doi.org/10.3390/ijms131216598.
[18] K. Ray, R. Badugu, J.R. Lakowicz, Metal-enhanced fluorescence from CdTe nanocrystals: a single-molecule fluorescence study, J. Am. Chem. Soc. 128 (2006) 8998–8999, http://dx.doi.org/10.1021/ja061762i.
[19] E. Dulkeith, M. Ringler, T.A. Klar, J. Feldmann, A. Muñoz Javier, W.J. Parak, Gold nanoparticles quench fluorescence by phase induced radiative rate suppression, Nano Lett. 5 (2005) 585–589, http://dx.doi.org/10.1021/nl0480969.
[20] J. Zhang, Y. Fu, M.H. Chowdhury, J.R. Lakowicz, Metal-enhanced single-molecule fluorescence on silver particle monomer and dimer: coupling effect between metal particles, Nano Lett. 7 (2007) 2101–2107, http://dx.doi.org/10.1021/nl071084d.
[21] M. Shanehsaz, A. Mohsenifar, S. Hasannia, N. Pirooznia, Y. Samaei, M. Shamsipur, Detection of *Helicobacter pylori* with a nanobiosensor based on fluorescence resonance energy transfer using CdTe quantum dots, Microchim. Acta 180 (2013) 195–202, http://dx.doi.org/10.1007/s00604-012-0906-2.
[22] Y.-P. Kim, Y.-H. Oh, E. Oh, S. Ko, M.-K. Han, H.-S. Kim, Energy transfer-based multiplexed assay of proteases by using gold nanoparticle and quantum dot conjugates on a surface, Anal. Chem. 80 (2008) 4634–4641, http://dx.doi.org/10.1021/ac702416e.
[23] A. Samanta, Y. Zhou, S. Zou, H. Yan, Y. Liu, Fluorescence quenching of quantum dots by gold nanoparticles: a potential long range spectroscopic ruler, Nano Lett. 14 (2014) 5052–5057, http://dx.doi.org/10.1021/nl501709s.
[24] D. Huang, C. Niu, M. Ruan, X. Wang, G. Zeng, C. Deng, Highly sensitive strategy for Hg 2^+ detection in environmental water samples using long lifetime fluorescence quantum dots and gold nanoparticles, Environ. Sci. Technol. 47 (2013) 4392–4398, http://dx.doi.org/10.1021/es302967n.
[25] M. Saponari, K. Manjunath, R.K. Yokomi, Quantitative detection of *Citrus tristeza virus* in citrus and aphids by real-time reverse transcription-PCR (TaqMan), J. Virol. Methods 147 (2008) 43–53, http://dx.doi.org/10.1016/j.jviromet.2007.07.026.
[26] T. Roodbar Shojaei, M.A. Mohd Salleh, K. Sijam, R. Abdul Rahim, A. Mohsenifar, R. Safarnejad, M. Tabatabaei, Fluorometric immunoassay for detecting the plant virus citrus tristeza using carbon nanoparticles acting as quenchers and antibodies labeled with CdTe quantum dots, Microchim. Acta 183 (2016) 2277–2287, http://dx.doi.org/10.1007/s00604-016-1867-7.
[27] A. Salomone, M. Mongelli, P. Roggero, D. Boscia, Reliability of detection of citrus tristeza virus by an immunochroma-tographic lateral flow assay in comparison with ELISA, J. Plant Pathol. 86 (2004) 43–48, http://dx.doi.org/10.4454/jpp.v86i1.936.
[28] S. Ruiz-Ruiz, P. Moreno, J. Guerri, S. Ambrós, A real-time RT-PCR assay for detection and absolute quantitation of citrus tristeza virus in different plant tissues, J. Virol. Methods 145 (2007) 96–105, http://dx.doi.org/10.1016/j.jviromet.2007.05.011.
[29] D.M. Mathews, K. Riley, J.A. Dodds, Comparison of detection methods for citrus tristeza virus in field trees during months of nonoptimal titer, Plant Dis. 81 (1997) 525–529, http://dx.doi.org/10.1094/PDIS.1997.81.5.525.
[30] Z. Huang, P.A. Rundell, X. Guan, C.A. Powell, Detection and isolate differentiation of citrus tristeza virus in infected field trees based on reverse transcription-polymerase chain reaction, Plant Dis. 88 (2004) 625–629, http://dx.doi.org/10.1094/PDIS.2004.88.6.625.
[31] M. Li, S.K. Cushing, Q. Wang, X. Shi, L.A. Hornak, Z. Hong, N. Wu, Size-dependent energy transfer between CdSe/ZnS quantum dots and gold nanoparticles, J. Phys. Chem. Lett. 2 (2011) 2125–2129, http://dx.doi.org/10.1021/jz201002g.
[32] W.P. Hall, S.N. Ngatia, R.P. Van Duyne, LSPR biosensor signal enhancement using nanoparticle-antibody conjugates, J. Phys. Chem. C. Nanomater. Interfaces 115 (2011) 1410–1414, http://dx.doi.org/10.1021/jp106912p.
[33] M. Zhou, I. Ghosh, Quantum dots and peptides: a bright future together, Biopolymers 88 (2007) 325–339, http://dx.doi.org/10.1002/bip.20655.